Available online at www.sciencedirect.com

ScienceDirect

Journal of Magnesium and Alloys 7 (2019) 240–248

www.elsevier.com/locate/jma

Full Length Article

Corrosion behavior of Mg–3Gd–1Zn–0.4Zr alloy with and without stacking faults

Xiaobo Zhang[a,*], Jianwei Dai[a], Ruifeng Zhang[b], Zhixin Ba[a], Nick Birbilis[c]

[a] *Jiangsu Key Laboratory of Advanced Structural Materials and Application Technology, School of Materials Science and Engineering, Nanjing Institute of Technology, Nanjing 211167, China*

[b] *School of Materials Science and Engineering, Central South University, Changsha 410083, China*

[c] *College of Engineering and Computer Science, Australian National University, Acton ACT 2000, Australia*

Received 3 January 2019; received in revised form 11 February 2019; accepted 16 February 2019
Available online 4 April 2019

Abstract

To develop biodegradable magnesium alloy with desirable corrosion properties, a low Gd-containing Mg–3Gd–1Zn–0.4Zr (wt%, GZ31K) alloy was prepared. The as-cast ingot was solution treated and then hot extruded. Microstructures were characterized by scanning electron microscopy (SEM). Corrosion behavior of the alloy under each condition was studied by hydrogen evolution and quasi in-situ corrosion methods. It has been found that the as-cast alloy is composed of α-Mg, stacking faults (SFs) at the outer edge of the matrix grains, and eutectic phase along the grain boundaries. After solution treatment, the SFs disappear and precipitates rich in Zn and Zr elements form in the grain interior and boundaries. The microstructure is significantly refined after extrusion. Hydrogen evolution tests show that the as-cast alloy exhibits the best corrosion resistance, and the solution-treated alloy has the worst corrosion resistance. Corrosion rate of the alloy under each condition decreases first and then increases with prolonging immersion time. Corrosion experiments demonstrate that α-Mg was corroded preferentially, the eutectic phase and precipitates exhibit better corrosion resistance. The as-extruded alloy demonstrates uniform corrosion due to fine and homogeneous microstructure.

Keywords: Magnesium alloys; Stacking faults; Corrosion resistance; Uniform corrosion.

1. Introduction

Biodegradable magnesium (Mg) alloys have attracted increasing attention in recent years for vascular stents, bone fixtures, and tissue engineering scaffolds applications due to their good biocompatibility, biodegradation, close density and modulus to human bones [1–3]. However, the main limitations to the application of Mg alloys as biodegradable implanted materials are their rapid corrosion rate and localized corrosion, which are detrimental to mechanical integrity during service [4–6].

Alloying is an effective method to enhance intrinsic corrosion resistance of Mg alloys if the kind and addition of alloying elements are suitable, as it could possible: (1) form a stable protective passive film on the alloy surface, (2) retard cathodic kinetics through poisoning hydrogen evolution reaction, (3) modify microstructure, form solid solution and even new intermetallics which act as cathodic sites and, (4) reduce the impurity tolerance limits in Mg [7]. Rare earth (RE) elements, such as Gd, Nd, Ho, Er, are popular alloying elements in biodegradable Mg alloys due to their good improvement on corrosion resistance [8–13]. It has been reported that Mg–6Ho–1Zn [12] and Mg–8Er–1Zn [13] alloys, with stacking faults (SFs) in different grains with various orientation, exhibit much better corrosion resistance as compared to those without SFs. We have lately reported a closer look at the role of SFs in the localized corrosion of Mg–3Gd–1Zn–0.4Zr alloy by quasi in-situ scanning transmission electron microscopy (STEM) prior to and following 1 min immersion

* Corresponding author.
E-mail address: xbzhang@njit.edu.cn (X. Zhang).

https://doi.org/10.1016/j.jma.2019.02.009

in NaCl solution [14]. It was indicated that the nanometer scale SFs, enriched in Gd and Zn, behaved as cathodic sites and protected from dissolution. And the periphery of the SFs was preferentially dissolved. Nevertheless, corrosion behavior of the alloy from a relative long-term was not referred.

In addition, as biomedical materials, the alloying elements should be non-toxicity. Gd has been confirmed to be acceptable toxic effect to primary cells and cell lines [15]. Mg–10Gd binary alloy shows no obvious toxicity to pre-osteoblast cells [16]. Zinc (Zn) and Zirconium (Zr) are common elements in biodegradable Mg alloys and show favorable cytocompatibility [17,18]. Our previous study has proven that Mg–11.3Gd–2.5Zn–0.6Zr alloy presents acceptable toxicity to L-929 cells [8]. Therefore, in this work, Mg–3Gd–1Zn–0.4Zr (wt%, GZ31K) alloy, which contains low Gd concentration and has SFs under as-cast condition [14], was selected as the aim alloy. The as-cast GZ31K alloy was solution treated (T4) and then hot extruded. Corrosion behavior of the alloy under as-cast, T4-treated, and as-extruded conditions was evaluated by quasi in-situ scanning electron microscopy and immersion methods.

2. Materials and methods

The as-cast GZ31K ingots, prepared by gravity casting [14], were hold at 535 °C for 12 h under a pyritic protective atmosphere, and then quenched into water to obtain T4-treated samples. The T4-treated rods were then hot extruded at 330 °C with an extrusion ratio of 9 and an extrusion ram speed of 0.5 mm/s. The specimens with a diameter of 14 mm and a thickness of 3 mm were cut, ground, and polished for microstructure observation, phase identification, and corrosion experiments.

A scanning electron microscope (SEM) coupled with an energy dispersive spectrometer (EDS) was used to observe microstructures of the as-cast, T4-treated, and as-extruded (perpendicular to extrusion direction) specimens. The grain size of the alloy was measured by linear intercept method. X-ray diffraction (XRD) was used to identify phases of the alloy under three conditions with a scanning rate of 10°/min.

To minimize the effects of other ions on corrosion behavior of the alloy, 0.1 M NaCl solution was adopted to immerse specimens. Quasi in-situ SEM was used to analyze the corrosion processes of the specimens prior to and following 5, 20, and 80 min immersion in 0.1 M NaCl solution. The EDS maps of Mg, Gd, Zn, Zr, and O were collected. Hydrogen (H_2) evolution tests were carried out in simulated body fluid (SBF) to evaluate corrosion rates of the specimens [19]. The H_2 volumes of each specimen were recorded every 24 h, then the SBF was renewed. The H_2 evolution tests lasted for 120 h and were quadruplicate for the alloy under three conditions to obtain average data. The corrosion morphologies after immersion in SBF for 120 h were observed by SEM prior to and following 5 min cleaning in 200 g/L CrO_3 solution, and the cross section of the immersed samples were also observed by SEM. The corrosion rates of the alloy were

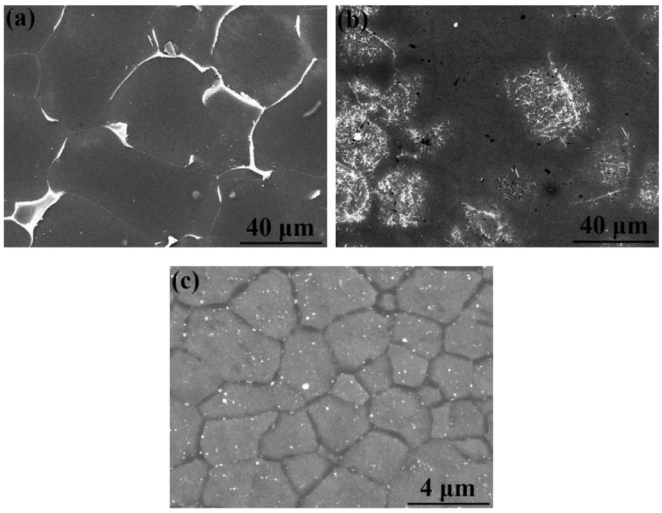

Fig. 1. Micrographs of the (a) as-cast, (b) T4-treated, and (c) as-extruded GZ31K alloys.

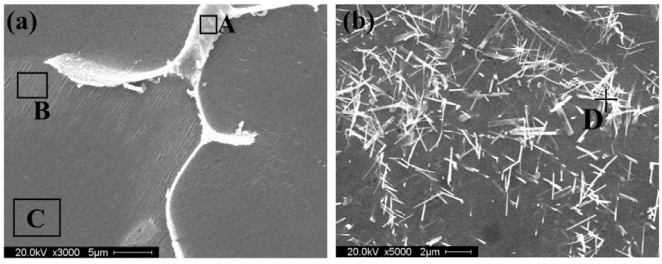

Fig. 2. High magnification SEM images of the (a) as-cast and (b) T4-treated GZ31K alloys.

calculated by the following formula [19]:

$$CR = \frac{95V_H}{A \times t \times \rho}$$

where CR is the corrosion rate (mm/year), V_H is the total volume of hydrogen evolution (mL), A is the surface area of the samples (cm^2), t is the immersion time (h), and ρ is the density of the alloys (g/cm^3).

3. Results and discussion

3.1. Microstructure and phase

Micrographs of the GZ31K alloy under various conditions are shown in Fig. 1. The as-cast alloy is composed of grey α-Mg, bright eutectic phase, and lamellar structures at the outer edge of α-Mg grains. After solution treated at 535 °C for 12 h, both eutectic phase and SFs are disappeared, and numerous needle-like precipitates are formed in grain interiors and grain boundaries. The as-extruded alloy is composed of equiaxed fine grains and tiny spherical particles, indicating the occurrence of dynamic recrystallization. The grain size of the as-cast, T4-treated, and as-extruded alloys are about 40 μm, 43 μm, and 3 μm, respectively.

Higher magnification micrographs are shown in Fig. 2 to present clearer lamellar structure and needle-like precipita-

Table 1
Chemical compositions (wt%) of different areas marked in Fig. 2.

Area	Gd	Zn	Zr	Mg
A	37.30	18.19	1.12	Bal.
B	9.25	3.95	2.58	Bal.
C	4.67	1.65	2.04	Bal.
D	3.86	3.51	4.24	Bal.

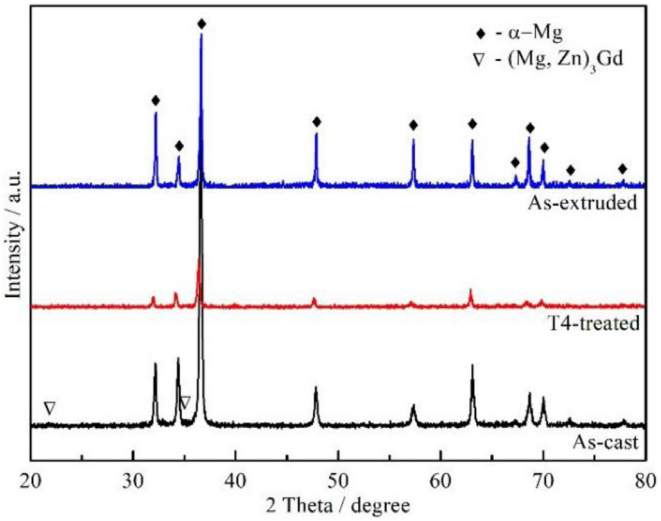

Fig. 3. XRD patterns of the GZ31K alloy under different conditions.

tions, and the compositions of different areas obtained by EDS are listed in Table 1. The lamellar structures are rich in Gd and Zn atoms, which have no long period stacking order and have been confirmed as stacking faults (SFs) by STEM [14]. The EDS results in Table 1 indicate that Gd and Zn concentrations in SFs are lower than those in eutectic phase but higher than those in α-Mg matrix. The needle-like precipitates are rich in Zr and Zn as compared to α-Mg matrix. XRD patterns (Fig. 3) show that α-Mg and $(Mg, Zn)_3Gd$ are detected in the as-cast alloy. Even though there are numerous needle-like precipitates in T4-treated alloy and spherical particles in as-extruded alloy, only α-Mg peaks are detected, which is mainly due to small volume fraction of precipitates.

SFs are often generated in Mg-RE-Zn systems, where RE corresponds to the following rare earth elements, Gd, Y, Ho, Er [12–14,20–24]. SFs in GZ31K alloy are rich in solute atoms of Gd and Zn. After being solution treated at 535 °C for 12 h, for the adequate dissolution, the eutectic phase $(Mg, Zn)_3Gd$ is dissolved completely, and the SFs are disappeared. Moreover, the needle-like particles are precipitated, which are often formed in heat-treated Mg–RE–Zn–Zr alloys and play a positive role in strengthening but a negative role in corrosion resistance [9,11,25–27]. Hot extrusion leads to a significant grain refinement due to dynamic recrystallization, and SFs are not visible from the SEM micrograph.

3.2. Corrosion behavior

Hydrogen evolution curves of the alloy immersed in SBF for 120 h are plotted in Fig. 4. It shows that the H_2 evolution

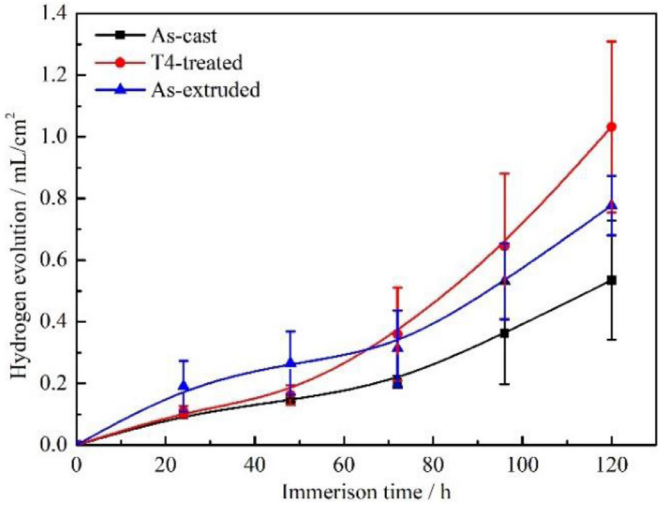

Fig. 4. H_2 evolution of the alloy in SBF following various immersion durations.

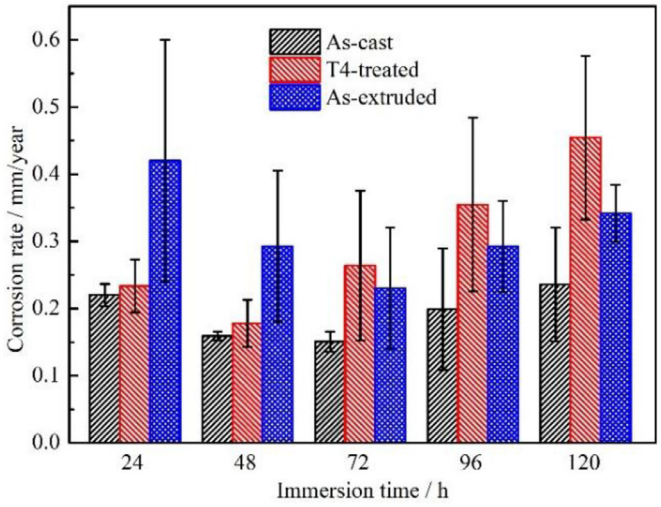

Fig. 5. Corrosion rates of the alloy in SBF calculated by H_2 evolution after various immersion durations.

volume of the as-cast alloy is the lowest for all immersion durations, that of the as-extruded alloy is the highest after immersion for 24 h and 48 h, and then presents a lower value than that of the T4-treated alloy. The total H_2 evolution volumes for 120 h immersion show that the as-cast alloy exhibits the highest corrosion resistance, and the T4-treated alloy has the lowest corrosion resistance. Moreover, the H_2 evolution volume of the as-extruded alloy is higher than that of the T4-treated one for 24 h and 48 h immersion, and then lowers for the following immersion, indicating that the as-extruded alloy suffers faster corrosion during the first 48 h immersion and slower corroison after then as compared to the T4-treated alloy.

In order to better present corrosion behavior of the alloy immersed in SBF for various durations, the corrosion rates of the alloy calculated by H_2 evolution volume after different immersion durations are shown in Fig. 5. It shows that the

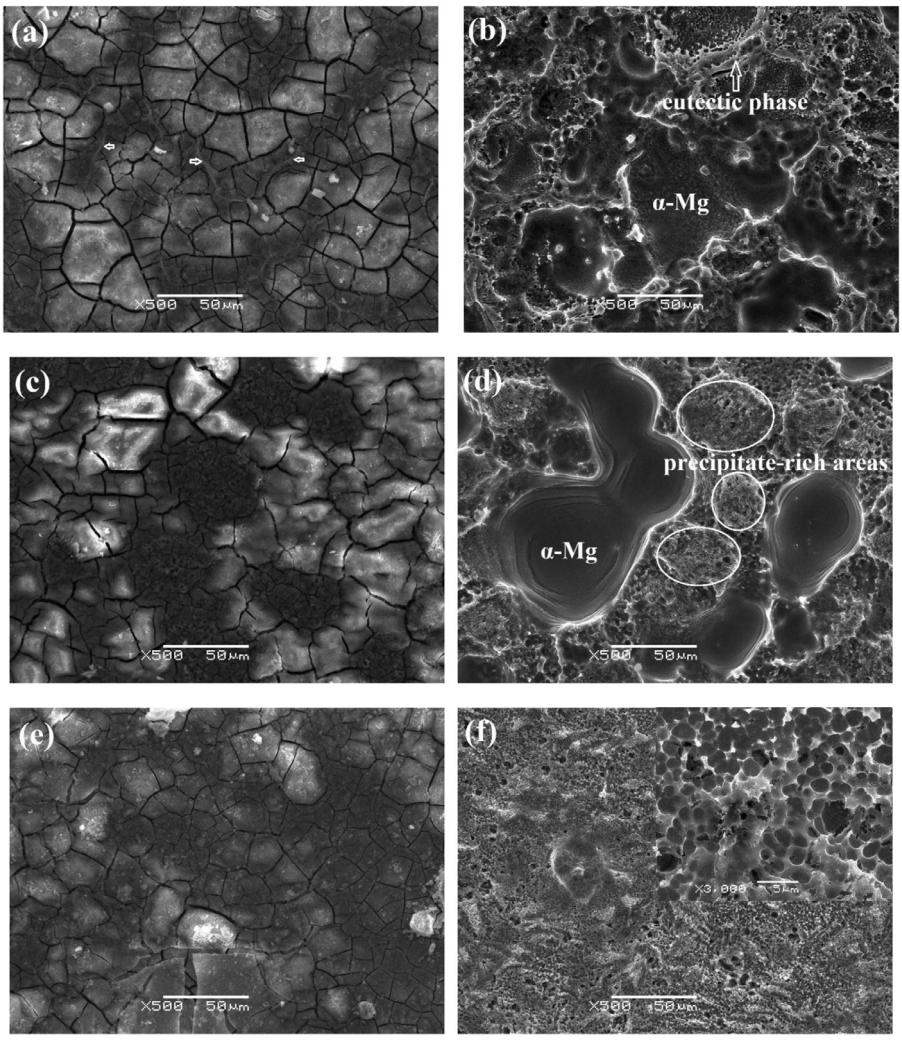

Fig. 6. Corrosion morphologies before (a, c, e) and after (b, d, f) cleaning corrosion products of the as-cast (a, b), T4-treated (c, d) and as-extruded (e, f) GZ31K alloys after 120 h immersion in SBF.

corrosion rates of the alloy under each condition decrease first and then increase with increasing immersion time. The lowest corrosion rates of the as-cast and as-extruded alloys are obtained after 72 h immersion, and the lowest corrosion rate of the T4-treated alloy is acquired after 48 h immersion. In general, the corrosion rates of the as-cast, T4-treated, and as-extruded GZ31K alloys after immerison in SBF for 120 h are 0.24, 0.45, and 0.34 mm/year, respectively, showing better corrosion resistance compared with Mg–5Gd–1Zn–0.6Zr alloy under the same condition [9,27,28].

Corrosion morphologies of the alloy prior to and following cleaning corrosion products are shown in Fig. 6. Microcracks are formed on the surfaces with corrosion products due to dehydration during drying the samples. The microcracks present wider width in the brighter areas where undergoes more corrosion. In addition, the eutectic phase configurations (as shown by arrows in Fig. 6(a)) are still visible, indicating better corrosion resistance. No serious macro corrosion pits are observed on the surfaces of the immersed samples after removing corrosion products, which demonstrates relatively uniform corrosion mode in macro range. Nevertheless, numerous tiny pits are found by SEM, as shown in Fig. 6(b), (d), and (f), revealing that the alloy undergoes pitting corrosion in micro range. It can be seen that α-Mg grains suffered more corrosion as compared to the eutectic phase and precipitate-rich areas in the as-cast and T4-treated alloys. These suggest that the eutectic phase and precipitates are more corrosion resistant than α-Mg matrix. The corroded morphology of the as-extruded alloy is the most uniform due to much finer and homogeneous microstructure.

The cross-section morphologies of the alloy after 120 immersion in SBF presented in Fig. 7 generally show that the T4-treated alloy has the most serious localized corrosion and the as-extruded alloy owns the most uniform corrosion. Moreover, the eutectic phase shown in Fig. 7(a) with black arrow also reveals that it is more corrosion resistant than α-Mg matrix, which is consistent with the corrosion morphology in Fig. 6(b). The arrows marked area in Fig. 7(b) are speculated for the α-Mg matrix without aggregated needle-like precipitates that can be inferred from Fig. 6(d).

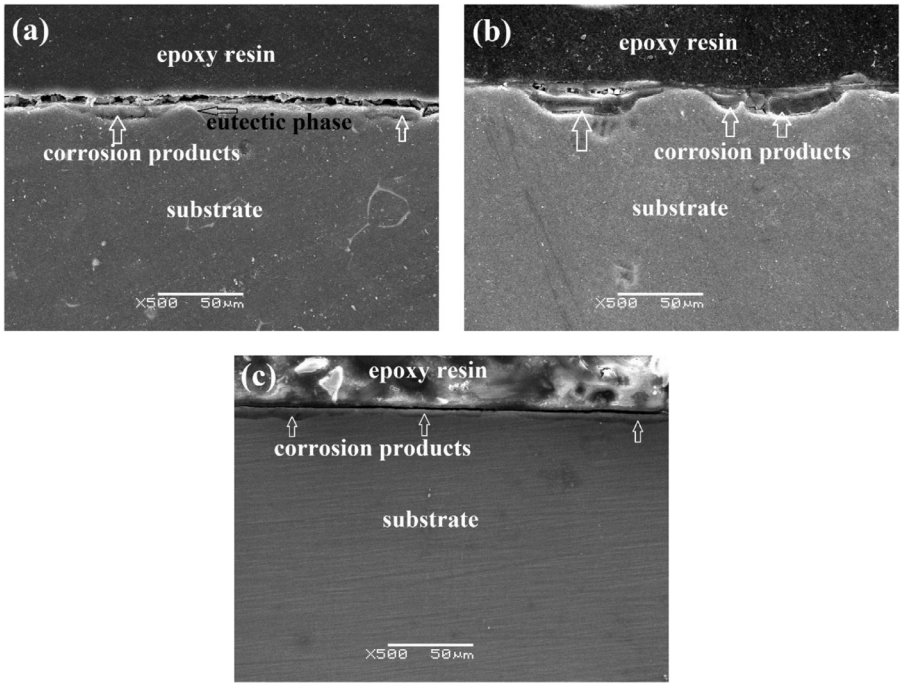

Fig. 7. Cross sections of the (a) as-cast, (b) T4-treated, and (c) as-extruded alloys after 120 h immersion in SBF.

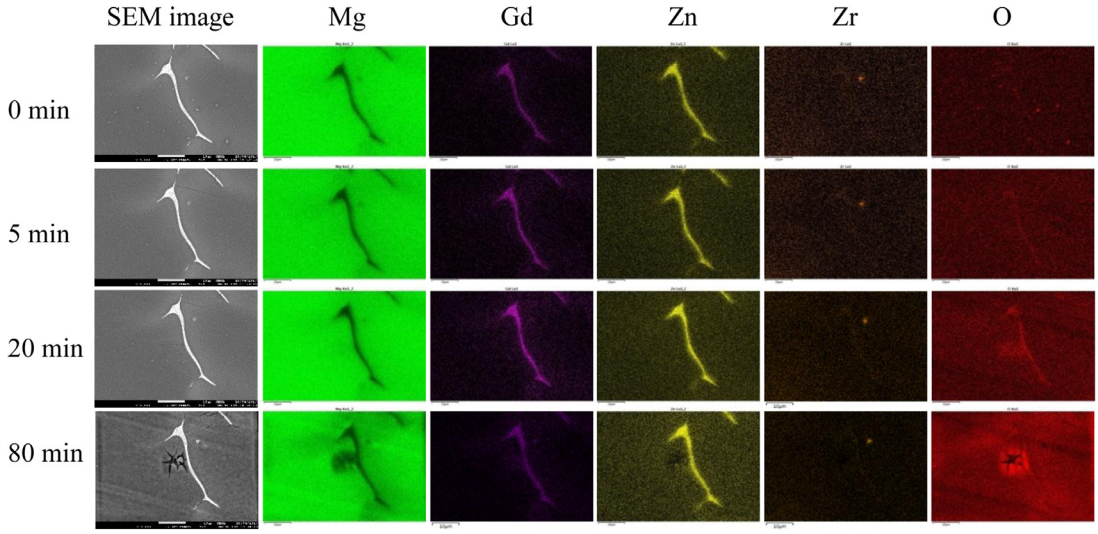

Fig. 8. SEM images and element distribution maps of the as-cast alloy following various immersion durations.

Quasi in-situ STEM corrosion of the as-cast GZ31K alloy after 1 min immersion in 0.1 M NaCl solution has been reported in Ref. [14]. Quasi in-situ corrosion tests were carried out using SEM to show corrosion process of the alloy under each condition for long-term. The SEM images and elements distribution of the as-cast, T4-treated, and as-extruded alloys following 0, 5, 20, and 80 min immersion in 0.1 M NaCl solution are shown in Figs. 8, 9, and 10, respectively.

As shown in Fig. 8, prior to immersion, the bright eutectic phase is rich in Gd and Zn elements. The SFs near the eutectic phase have more Gd and Zn than the matrix. Zr homogeneously distributes except for a Zr-rich particle. After 5 and 20 min immersion, no apparent corrosion is observed, and Mg, Gd, Zn, and Zr elements distribution presents no obvious difference. Nevertheless, more and more O element is detected particularly in the eutectic phase following 5 and 20 min immersion. After 80 min immersion, corrosion is apparently observed in the micrograph, particularly near the SFs. O element increases and Mg element reduces accordingly.

The eutectic phase is rich in Gd and Zn. According to our previous study, the corrosion potential of pure Gd is close to that of the GZ31K alloy, and the corrosion potential of pure Zn is much higher as compared to that of the GZ31K alloy [14]. Therefore, the aggregated O element on the eutectic phase is attributed to the oxidation of Gd, which has been also proved in Ref. [14].

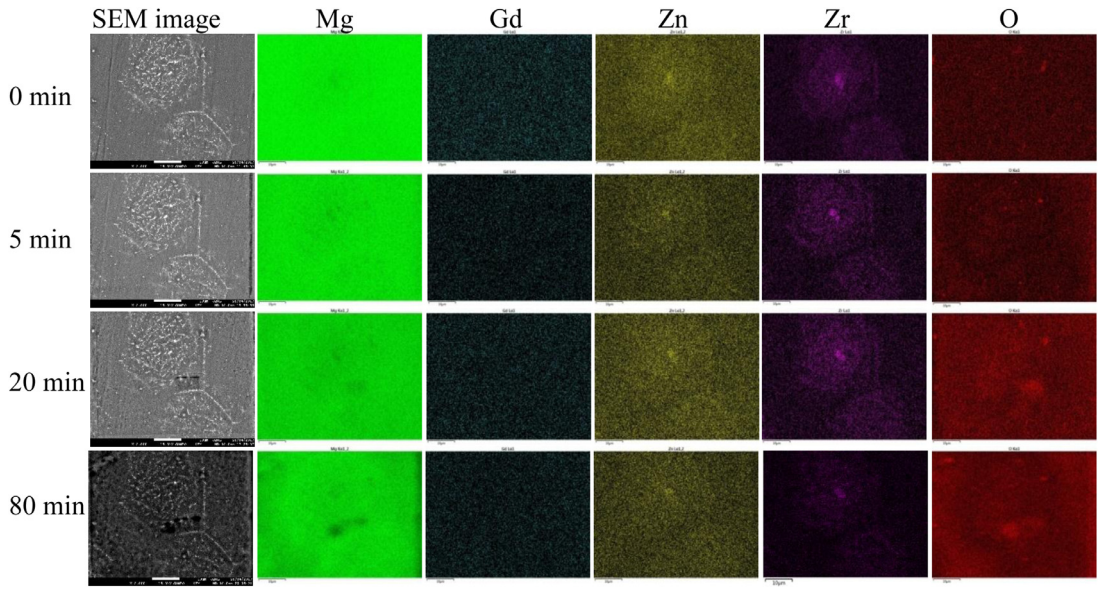

Fig. 9. SEM images and element distribution maps of the T4-treated alloy following various immersion durations.

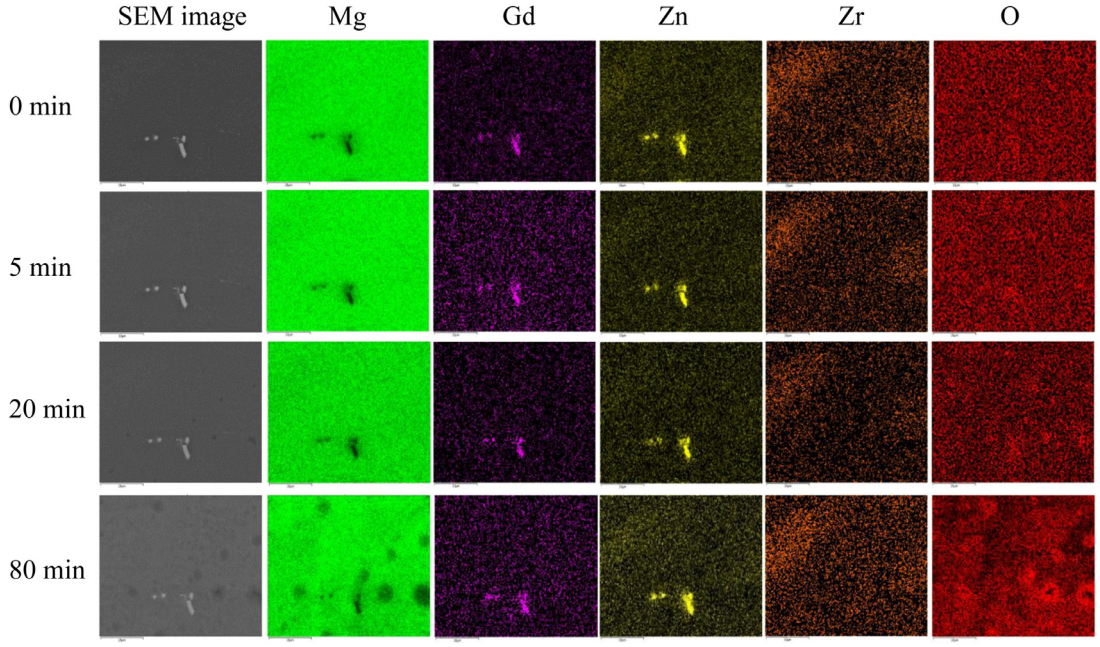

Fig. 10. SEM images and element distribution maps of the as-extruded alloy following various immersion durations.

It has been observed by STEM that α-Mg matrix is preferentially dissolved at the periphery of SFs following only 1 min immersion in 0.1 M NaCl solution due to galvanic corrosion [14]. For the long-term immersion (80 min), quasi in-situ SEM results indicate that the α-Mg matrix near the SFs and eutectic phase suffers severe corrosion, and the eutectic is the most corrosion resistant because it has the nobler corrosion potential and acts as cathode, while the α-Mg matrix exhibits the lowest corrosion potential and acts as anode.

As for the T4-treated alloy shown in Fig. 9, the eutectic phase dissolves into the matrix, and Gd element distributes uniformly. However, Zn and Zr elements are rich in the bright precipitates. Zn–Zr compounds are easily formed in T4-treated Mg–Gd–Zn–Zr alloys [9,25]. With increasing immersion time, the outer edge of the α-Mg matrix with less precipitates are gradually corroded. Mg and O elements show different distribution following 80 min immersion as compared to those following only 5 min. The Zn and Zr rich precipitates have been confirmed to be corrosion resistant phases and may cause local corrosion mode because of the formation of galvanic cell [9,11,25].

The quasi in-situ corrosion SEM images and element distribution maps of the as-extruded alloy are shown in Fig. 10. Precipitates, which are rich in Gd and Zn, are

observed, and they show no significant change following various immersion durations. With the increase of immersion time, Gd, Zn, and Zr elements show nonvisible difference, and the matrix preferentially undergoes corrosion, which is the same as the as-cast and T4-treated alloys.

Corrosion behavior of Mg alloys is significantly impacted by compositions and microstructures. In this work, the aimed alloy is Mg–3Gd–1Zn–0.4Zr alloy under as-cast, T4-treated, and as-extruded conditions, and hence, microstructure is the most important factor that dominates corrosion of the alloy. The microstructure of the as-cast GZ31K alloy is composed of α-Mg, discontinuous eutectic phase, and SFs at the outer edge of α-Mg grains. That of the T4-treated alloy is composed of α-Mg and precipitates rich in Zn and Zr elements, and the as-extruded alloy is composed of equiaxed fine grains and precipitates rich in Gd and Zn elements.

Generally, eutectic phase in Mg–Gd–Zn(–Zr) series alloy is regarded as cathode and accelerates matrix corrosion [29–31]. Nevertheless, some reports demonstrate that the Mg–Gd–Zn(–Zr) alloys with long period stacking ordered (LPSO) structure exhibit good corrosion resistance than those without LPSO structure even though they have eutectic phases along matrix grain boundaries [9,25,28,31,32]. This is because that the LPSO structure readily locates at the outer edge of matrix grains, and acts as corrosion barriers between matrix and eutectic phase, which can reduce microgalvanic corrosion between eutectic phase and LPSO, as well as LPSO and matrix [9,28,32]. Moreover, it has also been reported that the profuse SFs are beneficial to corrosion resistance of Mg–Ho–Zn and Mg–Er–Zn alloys [12,13]. On the one hand, corrosion expands along the length direction of the SFs, and the SFs in different grains exhibit different orientations. Hence, corrosion is hard to extend to the neighboring grains [12]. On the other hand, SFs are more active and dissolve first due to more energy than Mg matrix in Mg–Er–Zn alloy, and thus, the matrix grains are protected from corrosion [13]. In conclusion, LPSO and SFs play a significant role in corrosion resistance improvement of Mg alloys.

Moreover, tiny precipitates, which are often formed after heat treatment and plastic deformation, also impact corrosion resistance of Mg alloys [33–35]. It has been reported that finely distributed precipitates are beneficial to corrosion resistance of Mg–2Zn–21Gd–1Ca alloy [33] and lead to uniform corrosion due to their homogeneous distribution in Mg–Zn–Ca alloy [34]. Corrosion resistance of aged Mg–10Gd–5Y–2Zn–0.5Zr alloy was also improved by fine and uniformly distributed precipitates [35]. Nevertheless, tiny precipitates have also been confirmed to be detrimental to corrosion resistance of Mg–Gd–Zn–Zr [9,25] and Mg–Gd–Nd–Zn–Zr [11,36] alloys, which may also cause localized corrosion. In addition, grain size is another factor that influences corrosion resistance of Mg alloys. Most literature suggests that as grain size decreases, the corrosion resistance of Mg alloys is improved [37–40]. The enhanced corrosion resistance by grain refinement has been attributed to a better passive film [38].

In this work, the corrosion rate of the GZ31K alloy shows the following order after 120 h immersion in SBF: As-cast < as-extruded < T4-treated. As discussed above, eutectic phase always accelerates corrosion and fine grains often lead to the improvement of corrosion resistance. However, the as-cast GZ31K alloy exhibits better corrosion resistance even though it has eutectic phase and larger grains as compared to the as-extruded alloy. This is mainly attributed to the SFs at the outer edge of the matrix grains. As the quasi in-situ corrosion results show, the matrix grains are preferentially corroded. Furthermore, it has been directly illustrated that SFs are more corrosion resistant by STEM [14], more compact film would be formed after SFs being corroded and hence to protect the matrix from corrosion. Therefore, the SFs at the outer edge of grains effectively restrict corrosion from one grain to neighboring grains and retard corrosion, which act as the similar role to LPSO structure in Mg–Gd–Zn–Zr alloys containing higher Gd concentration [9,25,28]. The as-extruded alloy with much finer grains, however, has higher corrosion rate as compared to the as-cast one because of no SF prevention. The need-like precipitates and larger grains are possibly responsible for the highest rate and localized of corrosion of the T4-treated alloy among three conditions.

According to the corrosion results, the corrosion process schematic diagrams of the GZ31K alloy under each condition are presented in Fig. 11. As for the as-cast GZ31K alloy, α-Mg matrix is preferentially corroded due to the lowest corrosion potential, when corrosion spreads to the area containing SFs, the matrix between SFs corrodes, followed by the SFs. The eutectic phase, which has the noblest corrosion potential, is corroded lastly or peels off due to the complete corrosion around it. Because of the formation of SFs at the outer edge of matrix grains, the as-cast GZ31K alloy exhibits relatively uniform corrosion. As for the T4-treated alloy, the α-Mg grains with less precipitates are corroded preferentially and the precipitate-rich areas are protected for the noble corrosion potential as cathode. Since there is no continuous corrosion barrier, the T4-treated alloy undergoes apparent localized corrosion. The same to the as-cast and T4-treated alloy, the preferential corrosion in the as-extruded GZ31K alloy is also occurred in the α-Mg grains, followed by the tiny particles. The fine and uniform grains, including matrix grains and precipitates, lead to uniform corrosion mode.

It is notable that the corrosion rates of the alloy under each condition decrease first then increase with increasing immersion time during 120 h immersion test. A formation of corrosion product layer may be the reason that influences the corrosion rate as the immersion time went on. At the early stage of immersion, the corrosion products deposited on the surface of the specimen. As the immersion time increases, the layer became thicker and compacter, which could play a protective film and protect the substrate from corrosion enhanced [41,42]. The corrosion layer would become loose and even peel off with further increasing immersion time, as a result, the corrosion rate of increases [43]. Similar results have also been found in as-cast and T4-treated GZ60K alloy [25].

It should be also mentioned that as biodegradable implants, both high strength and good corrosion resistance are desired for Mg alloys since these can provide sufficient mechanical

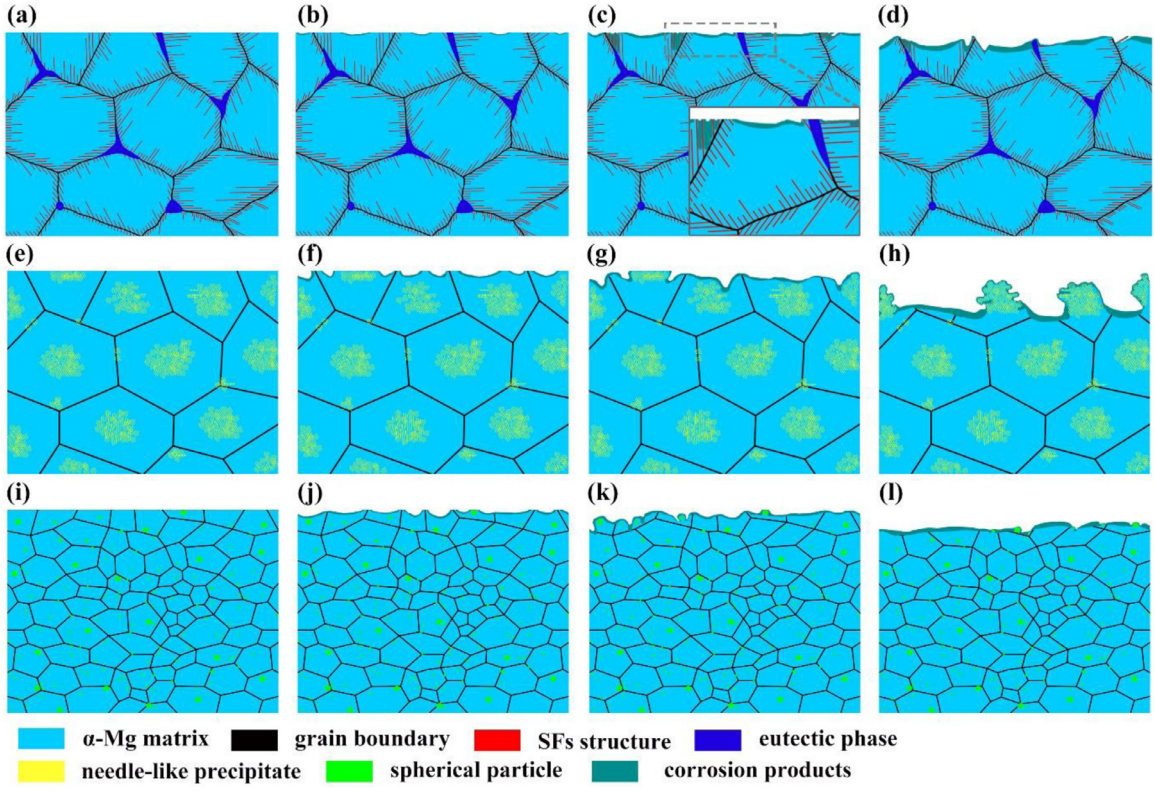

Fig. 11. Schematic diagrams showing corrosion processes of GZ31K alloy under different conditions (a–d) as-cast alloy, (e–h) T4-treated alloy, and (i–l) as-extruded alloy.

support before the disease is healed. It is well known that hot deformed Mg alloys have much higher mechanical properties as compared to the as-cast ones [27,44–46], and the mechanical properties of the as-extruded GZ31K is much higher than those of the as-cast alloy which will be published elsewhere. However, the as-cast alloy shows better corrosion resistance than the as-extruded GZ31K alloy which is mainly attributed to the formation of stacking faults. According to our latest research, the SFs have been found in the as-extruded GZ60K and GZ61K alloys. Profuse SFs have also been observed in many other hot deformed Mg alloys [12,13,23,24]. Consequently, revealing the stability of SFs and then keeping stacking faults in the as-extruded GZ31K alloy to acquire both high strength and high corrosion resistance are worthy of further study.

4. Conclusions

(1) The as-cast Mg–3Gd–1Zn–0.4Zr alloy consists of α-Mg, stacking faults at the outer edge of the matrix grains, and eutectic phase. Following solution treatment at 535 °C for 12 h, the T4-treated alloy is composed of α-Mg and needle-like precipitates. The as-extruded alloy is composed of fine equiaxed grains and precipitates rich in Gd and Zn elements.

(2) Hydrogen evolution tests demonstrate that the Mg–3Gd–1Zn–0.4Zr alloy under three conditions shows the following corrosion resistance: As-cast > as-extruded > T4-treated.

(3) α-Mg in the Mg–3Gd–1Zn–0.4Zr alloy under each condition is found to be corroded preferentially, eutectic phases and precipitates exhibit better corrosion resistance.

(4) The GZ31K alloy exhibits the following trend from uniform to localized corrosion: As-extruded > as-cast > T4-treated.

Conflict of Interest

None.

Acknowledgment

This project was supported by the Natural Science Foundation of Jiangsu Province for Outstanding Youth (BK20160081), the Natural Science Foundation of Higher Education Institutions of Jiangsu Province – Key Project (18KJA430008), the Jiangsu Government Scholarship for Overseas Studies, the “333 Project” of Jiangsu Province (BRA2018338), the National Natural Science Foundation of China (51701093), and the Outstanding Scientific and Technological Innovation Team in Colleges and Universities of Jiangsu Province.

References

[1] F. Witte, N. Hort, C. Vogem, S. Cohen, K.U. Kainer, R. Willumeit, F. Feyerabend, Curr. Opin. Solid State Mater. Sci. 12 (2008) 63–72.
[2] Y. Chen, Z. Xu, C. Smith, J. Sankar, Acta Biomater. 10 (2014) 4561–4573.
[3] N. Sezer, Z. Evis, S.M. Kayhan, A. Tehmasebifar, M. Koç, J. Magnes. Alloys 6 (2018) 23–43.
[4] G. Zhang, L. Wu, A. Tang, Y. Ma, G. Song, D. Zheng, B. Jiang, A. Atrens, F. Pan, Corros. Sci. 139 (2018) 370–382.
[5] J. Dai, X. Zhang, Q. Yin, S. Ni, Z. Ba, Z. Wang, J. Magnes. Alloys 5 (2017) 448–453.
[6] L. Wu, D. Yang, G. Zhang, Z. Zhang, S. Zhang, A. Tang, F. Pan, Appl. Surf. Sci. 431 (2018) 177–186.
[7] F. Cao, G. Song, A. Atrens, Corros. Sci. 111 (2016) 835–845.
[8] X. Zhang, Y. Wu, Y. Xue, Z. Wang, L. Yang, Mater. Lett. 86 (2012) 42–45.
[9] X. Zhang, Z. Ba, Q. Wang, Y. Wu, Z. Wang, Q. Wang, Corros. Sci. 88 (2014) 1–5.
[10] J. Niu, M. Xiong, X. Guan, J. Zhang, H. Huang, J. Pei, G. Yuan, Corros. Sci. 113 (2016) 183–187.
[11] X. Zhang, Y. Xue, Z. Wang, X. He, Q. Wang, Acta Metall. Sin. 50 (2014) 979–988.
[12] L. Zhang, J. Zhang, C. Xu, Y. Jing, J. Zhuang, R. Wu, M. Zhang, Mater. Lett. 133 (2014) 158–162.
[13] J. Zhang, C. Xu, Y. Jing, S. Lv, S. Liu, D. Fang, J. Zhuang, M. Zhang, R. Wu, Sci. Rep. 5 (2015) 13933.
[14] X. Zhang, S.K. Kairy, J. Dai, N. Birbilis, J. Electro. Soc. 165 (2018) C310–C316.
[15] F. Feyerabend, J. Fischer, J. Holtz, F. Witte, R. Willumeit, H. Drücher, C. Vogt, N. Hort, Acta Biomater. 6 (2010) 1834–1842.
[16] A. Myrissa, N.A. Agha, Y. Lu, E. Martinelli, J. Eichler, G. Szakács, C. Kleinhans, R. Willumeit-Römer, U. Schäfer, A.M. Weinberg, Mater. Sci. Eng. C 61 (2016) 865–874.
[17] D. Hong, P. Saha, D.T. Chou, B. Lee, B.E. Collins, Z. Tan, Z. Dong, P.N. Kumta, Acta Biomater. 9 (2013) 8534–8547.
[18] Z. Huan, M.A. Leeflang, J. Zhou, L.E. Fratila-Apachitei, J. Duszczyk, J. Mater. Sci: Mater. Med. 21 (2010) 2623–2635.
[19] K. Chen, X. Zhang, J. Dai, Y. Fei, Z. Wang, Mater. Technol. 31 (2016) 210–215.
[20] M. Yamasaki, M. Sasaki, M. Nishijima, K. Hiraga, Y. Kawamura, Acta Mater. 55 (2007) 6798–6805.
[21] J. Lee, K. Sato, T.J. Konno, K. Hiraga, Mater. Trans. 50 (2009) 222–225.
[22] J. Zhang, Z. Leng, S. Liu, J. Li, M. Zhang, R. Wu, J. Alloys Compd. 509 (2011) 7717–7722.
[23] Y. Jiao, J. Zhang, Y. Jing, C. Xu, S. Liu, L. Zhang, L. Xu, M. Zhang, R. Wu, Adv. Eng. Mater. 17 (2015) 876–884.
[24] C. Xu, T. Nakata, X. Qiao, M. Zheng, K. Wu, S. Kamado, Sci. Rep. 7 (2017) 40846.
[25] X. Zhang, Z. Ba, Z. Wang, Y.J. Xue, Corros. Sci. 105 (2016) 68–77.
[26] J. Zhang, X. Zhang, Q. Liu, S. Yang, Z. Wang, J. Mater. Sci. Technol. 33 (2017) 645–651.
[27] X. Zhang, Z. Ba, Z. Wang, Y. Wu, Y Xue, Mater. Lett. 163 (2016) 250–253.
[28] X. Zhang, Q. Wang, F. Chen, Y. Wu, Z. Wang, Q. Wangy, Mater. Lett. 138 (2015) 212–215.
[29] A. Srinivasan, C. Blawert, Y. Huang, C.L. Mendis, K.U. Kainer, N. Hort, J. Magnes. Alloys 2 (2014) 245–256.
[30] X. Zong, D. Wang, W. Liu, K. Nie, C. Xu, J. Zhang, Acta Metall. Sin. 29 (2016) 32–38.
[31] J. Zhang, D. Wang, W. Zhang, H. Pei, Z. You, C. Xu, W. Cheng, Mater. Corros. 66 (2015) 542–548.
[32] J. Wang, W. Jiang, Y. Ma, Y. Li, S. Huang, Mater. Chem. Phys. 203 (2018) 352–361.
[33] M. Janbozorgi, K.K. Taheri, A.K. Teheri, J. Magnes. Alloys. 7 (2019) 80–89, doi:10.1016/j.jma.2018.11.002.
[34] J. Gao, S. Guan, Z. Ren, Y. Sun, S. Zhu, B. Wang, Mater. Lett. 65 (2011) 691–693.
[35] Y. Zou, X. Chen, B. Chen, J. Mater. Res. 33 (2018) 745–757.
[36] Y. Liu, Z. Kang, L. Zhou, J. Zhang, Y. Li, Corros. Eng. Sci. Technol. 51 (2016) 256–262.
[37] C. op'tHong, N. Birbilis, Y. Estrin, Adv. Eng. Mater. 10 (2008) 579–582.
[38] K.D. Ralston, B. Birbilis, Corrosion 66 (2010) 075005.
[39] X. Zhang, Q. Ma, Z. Ba, Z. Wang, Q. Wang, Rare Met. Mater. Eng. 46 (2017) 1156–1161.
[40] Z. Gui, Z. Kang, Y. Li, J. Alloys Comp. 685 (2016) 222–230.
[41] D. Liu, Y. Liu, Y. Huang, R. Song, M. Chen, Pro. Nat. Sci. Mater. Inter. 24 (2014) 452–457.
[42] R. Guan, A.F. Cipriano, Z. Zhao, J. Lock, D. Tie, T. Zhao, T. Cui, H. Liu, Mater. Sci. Eng. C 33 (2013) 3661–3669.
[43] X. Zhang, J. Dai, H. Yang, S. Liu, X. He, Z. Wang, Mater. Technol. 32 (2017) 399–408.
[44] H. Yao, J. Wen, Y. Xiong, Y. Lu, F. Ren, W. Cao, J. Alloys Comp. 739 (2018) 468–480.
[45] T. Motoyama, H. Watanabe, N. Ikeo, T. Mukai, Mater. Lett. 201 (2017) 144–147.
[46] Y. Ding, Q. Le, Z. Zhang, J. Cui, J. Mater. Pro. Technol. 233 (2016) 161–173.